Available online at www.sciencedirect.com
ScienceDirect
Journal of Catalysis 248 (2007) 77–88
JOURNAL OF CATALYSIS
www.elsevier.com/locate/jcat

A computer modeling study of redox processes on the $FeSbO_4$ (100) surface

Ricardo Grau-Crespo [a,b,*], C. Richard A. Catlow [b,c], Nora H. de Leeuw [a,b]

[a] *School of Crystallography, Birkbeck College, University of London, Malet Street, London, WC1E 7HX, UK*
[b] *Department of Chemistry, University College London, 20 Gordon Street, London, WC1H 0AJ, UK*
[c] *Davy Faraday Research Laboratory, The Royal Institution of Great Britain, 21 Albemarle Street, London, W1X 4BS, UK*

Received 4 December 2006; revised 16 February 2007; accepted 19 February 2007

Abstract

Computer modeling techniques, based on the density functional theory, were used to investigate the oxidation–reduction behavior of the (100) surface of iron antimony oxide, $FeSbO_4$. We calculated the geometries and stabilities of different surface compositions with deficiency or excess of oxygen and also with two different distributions of cations, a bulk-like distribution with Fe and Sb alternation in the [001] direction and a segregated distribution with an Sb-rich surface. We found that the creation of oxygen vacancies in the surface led to the formation of surface Sb^{3+} species, with lone pairs pointing at the vacancy site. The electrons localized on the iron to form Fe^{2+} species only if there were no Sb^{5+} cations present to reduce preferentially. The formation of oxygen vacancies was more favorable on the Sb-segregated surface than on the nonsegregated surface because of the strong relaxation that occurs in the former on vacancy formation. Molecular oxygen can adsorb at an oxygen vacancy in the form of a peroxy ion, taking the electrons from the reduced Sb^{3+} cation near the vacancy. But this adsorbed peroxy species is only metastable, as the oxidized surface is thermodynamically unfavorable with respect to the stoichiometric surface.

Keywords: Iron antimonate; Oxygen vacancies; Surface reduction; Selective oxidation; Cation segregation; Peroxy; Ab initio thermodynamics; DFT

1. Introduction

Over the last few decades, the iron antimony oxide $FeSbO_4$ has attracted considerable interest as the main component of several industrial catalysts for the selective oxidation of propene and other hydrocarbons [1–5]. These processes have significant industrial relevance, because they produce about one-quarter of the organic precursor chemicals and intermediates used in the manufacture of further industrial products and consumer goods, including acrolein, acrylic acid, acrylonitrile, methacrylic acid, MTBE (methyl tertiary butyl ether), maleic anhydride, phtalic anhydride, ethylene and propylene oxide [6].

At present, there is no consensus as to the exact processes occurring on the surface of the antimonate catalysts during these reactions. For example, it was recognized early on that the selectivity for partial oxidation of Fe–Sb–O catalysts is improved significantly when the catalyst is prepared with Sb in excess of the Sb/Fe = 1 composition corresponding to $FeSbO_4$ [7,8], but the explanation for this effect is still the subject of long-standing debate [9–17].

The structure of the pure $FeSbO_4$ phase can be described in terms of a rutile-like framework with Fe and Sb cations distributed in the octahedral sites within the oxygen lattice. Although some diffraction data have been interpreted in terms of partial cationic ordering in a trirutile structure (triple *c* parameter compared with normal rutile), most experimental studies have concluded that the cation distribution is completely disordered (see Ref. [18] for a review). However, a recent computer modeling study [19] of the distribution of cations in the crystal structure showed that Fe and Sb cations have a clear energetic preference to alternate along the *c*-axis of the crystal, while these chains of alternating cations connect laterally with significant disorder in the *a*–*b* plane, which prevents three-dimensional long-range ordering. This calculated, one-dimensional cation ordering is in good agreement with experimental evidence of the magnetic properties of the material. According to neutron diffraction studies [20], the magnetic correlations extend in the *a* and *b* directions of the crystal, but not in the *c* direction, which

* Corresponding author.
E-mail address: r.grau-crespo@ucl.ac.uk (R. Grau-Crespo).

0021-9517/$ – see front matter
doi:10.1016/j.jcat.2007.02.015

is likely to be a consequence of the preferential alternation of magnetic (Fe^{3+}) and nonmagnetic (Sb^{5+}) cations in that direction [21].

In a previous study, [22] we investigated the formation of oxygen vacancies in the bulk of iron antimonate and the effect of the cation distribution on the properties of the vacancy, and found a significant variation in the stability and electronic properties of oxygen vacancies depending on their cation coordination in the mixed oxide; the higher the number of Sb atoms around the oxygen, the greater the energy of formation of the vacancy from the corresponding parent structure. We also found that the electrons remaining after oxygen abstraction preferably localize on Sb rather than Fe, forming electron lone pairs that orientate toward the vacancy site.

In the present work, we investigated the formation of vacancies at the $FeSbO_4$ surface, because in the selective oxidation process, the oxygen for the catalytic reactions is taken from the surface, which is then reoxidized by oxygen in the gas phase. We focus on the properties of the (100) surface, which appears to be the most prominent surface of $FeSbO_4$ [23]. We study the surface reduction via the formation of oxygen vacancies and the adsorption of oxygen on the surface and explore how the feasibility of these processes is determined by the conditions of temperature and oxygen partial pressure. We also discuss the effect of the segregation of the cations to form an Sb-rich surface on the oxidation–reduction behavior of the surface. We note that the problem addressed here is of key importance generally in oxidation catalysis effected by mixed metal oxides.

2. Methodology

2.1. Calculation details

We performed spin-polarized quantum mechanical calculations based on density functional theory (DFT) in the plane-wave pseudopotential formulation, using the Vienna Ab Initio Simulation Program (VASP) [24–27]. Although the local density (LDA) and the generalized gradient (GGA) approximations are generally used within periodic DFT, these are known not to describe the electronic properties of early transition metal (TM) compounds properly; the electron self-interaction error always present in these formulations becomes significant for electrons in the well-localized TM *d* levels. In these cases, the total energy can also be affected, because the error is introduced due to the failure of the energy functional in dealing with electron self-interaction. Therefore, the prediction of energy differences also can also be very poor in cases in which charge transfer occurs involving *d* orbitals. In the present study, where we are concerned with redox processes involving Fe^{3+} among other cations, we used an alternative approach, the so-called DFT + U methodology [28–31], which combines the DFT and a Hubbard Hamiltonian to account for the intra-atomic Coulomb repulsion, which is not well described in standard DFT. The DFT + U correction acts by altering the one-electron potential locally for the specified orbitals of the metal atoms (e.g., Fe *d* orbitals), reducing the hybridization with the ligands (e.g., O atoms). Here we use the simple DFT + U formulation of Liechtenstein et al. [30] and Dudarev et al. [31], where a single parameter, U_{eff}, determines an orbital-dependent correction to the DFT energy. U_{eff} is generally expressed as the difference between two parameters, the Hubbard U, which is the Coulomb-energetic cost of placing two electrons at the same site, and an approximation of the Stoner exchange parameter I, which is almost constant at ∼1 eV [32], and the $U_{\text{eff}} = 0$ case represents the DFT limit. Details of the implementation of the DFT + U method in the VASP code can be found elsewhere [29].

The DFT solution within the DFT + U approach can be obtained at either the LDA or GGA level, giving rise to what have been called the LDA + U and the GGA + U formulations, respectively (see Ref. [29] for a comparison between the two formulations). Here we used the GGA + U approximation with a GGA functional built from the Perdew and Zunger [33] local functional, with the spin interpolation formula of Vosko et al. [34] and the gradient corrections of Perdew et al. [35]. The DFT + U method has a number of limitations, perhaps the most important of which is the difficulty in choosing an adequate value for the U_{eff} parameter. A typical approach involves taking U_{eff} as an empirical parameter and fitting its value to reproduce certain experimental observables, but optimum values usually are property-dependent [29,36], which is clearly unsatisfactory. Despite these limitations, the DFT + U approach can be very useful, when applied with care and checked thoroughly, in the investigation of systems in which traditional DFT becomes unworkable.

In a previous paper [37], we extensively investigated the validity of the DFT + U approach in the description of $FeSbO_4$ bulk properties compared with traditional DFT and with hybrid DFT/Hartree–Fock functionals. It was shown that the GGA + U methodology with $U_{\text{eff}} = 4$ eV provides an adequate description of the electronic structure and the magnetic interactions in this oxide, in contrast with pure GGA, which predicts too high a magnetic coupling, too narrow a band gap, and a pressure-induced Fe spin transition with no experimental support. The validity of the GGA + U approach also has also been shown in surface calculations for other transition metal oxides. Rohrbach et al. [38] compared the GGA + U and the pure GGA approaches in modeling the (0001) surfaces of hematite (Fe_2O_3) and chromia (Cr_2O_3) and found that electron self-interaction errors have a dramatic influence on the surface stability and that for both oxides, the inclusion of the U correction for the transition metal *d* orbitals led to greater stability of the stoichiometric metal-terminated surface with respect to the oxidized surface even under strongly oxidizing conditions, in good agreement with scanning tunneling microscopy (STM) and low-energy electron diffraction (LEED) data. Therefore, we used the GGA + U methodology in all of our calculations, with the same value of the U_{eff} parameter (4 eV) that was previously found to describe best the properties of the $FeSbO_4$ bulk material.

The interaction between the valence electrons and the core was described with the projected augmented wave (PAW) method [39] in the implementation of Kresse and Joubert [40]. The number of plane waves in VASP is controlled by the cutoff

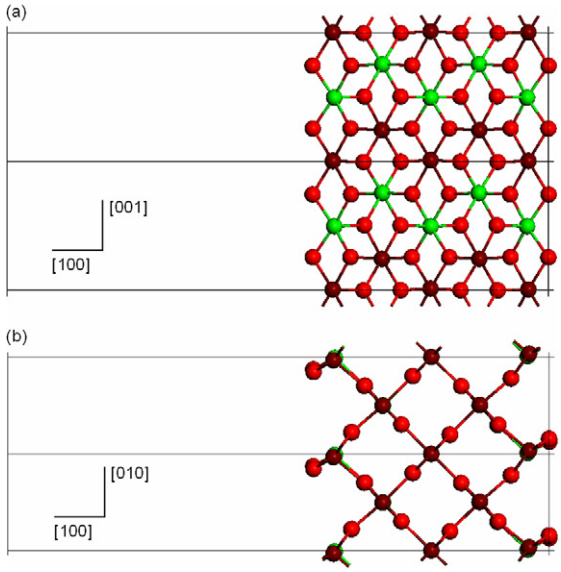

Fig. 1. Supercell model (doubled in each surface direction) for the relaxed stoichiometric (100) surface of $FeSbO_4$. (a) View along the [010] direction; (b) view along the [001] direction. Red, brown and green represent oxygen, iron and antimony, respectively. The cations are distributed in the surface as in the perfect bulk arrangement, with Fe and Sb alternating along the [001] direction. (For interpretation of the references to colour in this figure legend, the reader is referred to the web of this article.)

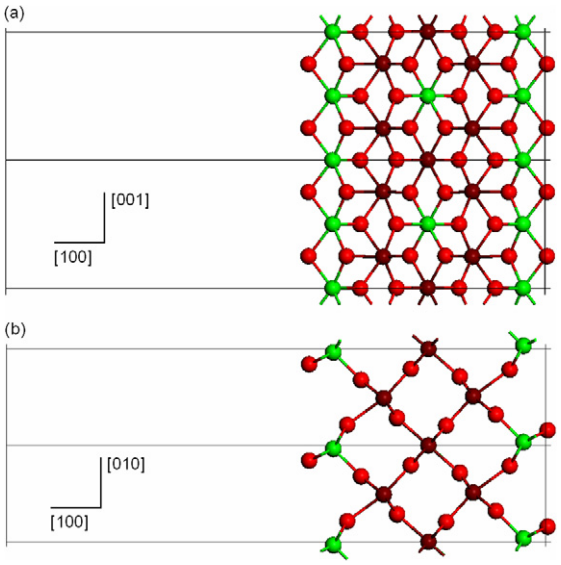

Fig. 2. Relaxed Sb-segregated (100) surface of overall stoichiometric composition. (a) View along the [010] direction; (b) view along the [001] direction. Red, brown and green represent oxygen, iron and antimony, respectively.

energy, which in all of our calculations was $E_{cut} = 400$ eV, as determined by a series of test calculations to check the convergence of energies and lattice parameters.

2.2. Surface models

Our slab model for the (100) surface of $FeSbO_4$ consists of five layers of octahedra (5 $FeSbO_4$ formula units, or 30 atoms in total) along the [100] direction and 1×2 periodicity parallel to the surface (Fig. 1). The double cell along the [001] direction enables the alternation of Fe and Sb cations in this direction, in agreement with previous findings for the bulk structure [19,21]. However, here we also explore the possibility of a different cation arrangement in the surface compared with the ideal bulk distribution. Fig. 2 shows a slab model in which the surface layer contains only Sb cations and the subsurface layer contains only Fe cations, whereas the central layer remains mixed. We use this model to explore the effect of Sb segregation on the surface properties, as this is a topic of interest for the understanding of the catalytic properties of iron antimonate; several authors have reported that the best selectivities in alkene oxidation reactions are obtained when the surface of $FeSbO_4$ is enriched in Sb [7,9,12], and it has been shown that synthetic $FeSbO_4$ particles have an Sb-rich surface, although it is unclear whether this is due to thermodynamically favored Sb segregation or simply to incomplete volatilization of antimony oxide from the system during sample preparation [41].

In both cases, the two surfaces of the slab are symmetrically equivalent, because the structure has a two-fold rotation axis oriented along the [001] direction. This symmetry is kept during all of the calculations, ensuring that both surfaces are always identical, thus preventing the formation of the electric dipole moments that are usually associated with asymmetric slabs, which requires compensation if the calculated structures and energies are to be valid.

Due to the use of three-dimensional periodic boundary conditions, this type of model yields the energy and properties of an array of crystal slabs. To ensure that the results of the calculation correctly represent the isolated surface, the vacuum regions must be sufficiently wide so that the faces of adjacent crystal slabs do not strongly interact across the vacuum region, and the crystal slab must be sufficiently thick so that the two surfaces of each crystal slab do not interact through the bulk crystal. In our case, the vacuum gap is ∼15 Å, and we have checked that for the nonsegregated slab model, an increase to 18 Å produces a change in the total energy of only 1 meV.

The choice of slab thickness is more problematic, because the cost of the calculations increases significantly more with the size of the slab than with the width of the vacuum gap. We verified that the variation of the surface energy (see the next section) of the unsegregated stoichiometric surface when increasing the slab thickness from 5 to 7 octahedral layers is <0.2%, which is certainly negligible. However, the fact that this slab thickness is sufficient to calculate the surface energy of the stoichiometric surface does not guarantee that it will be sufficient for investigation of the redox behavior of the surface. In these cases, a strong relaxation or reconstruction of the surface may occur, and the interactions between the two surfaces of the slab may be appreciable. This issue is discussed in more detail in the following sections.

Another aspect meriting consideration is the ordering of the Fe^{3+} magnetic moments in the slab. For the nonsegregated surface, we have assumed that the same antiferromagnetic ordering of the bulk is kept in the slab. Because of the odd number of magnetic atoms, this ordering means that the total difference between the numbers of α-spin and β-spin electrons in the stoichiometric slab will be 5, which corresponds to the number of

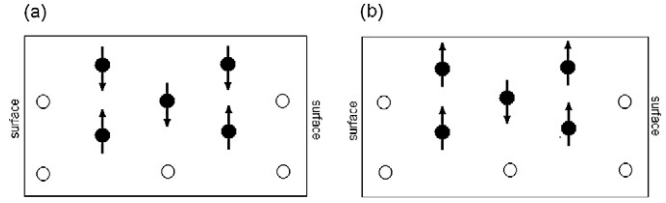

Fig. 3. The two different orientations of the Fe^{3+} magnetic moments in the slab with Sb segregation: (a) all vertical pairs have antiparallel spins, (b) all diagonal pairs have antiparallel spins. Solid circles are Fe cations; open circles are Sb cations; oxygen anions are omitted.

unpaired electrons in one high-spin Fe^{3+} ion. Within the VASP code, it is possible to assign an initial spin population and orientation at each atom, and the system will converge to the ground state spin configuration, but keeping the same orientation of the spins. We checked whether the calculation of the stoichiometric slab converges to the correct total number of unpaired electrons when this number is not fixed.

On the other hand, there are both vertical and diagonal magnetically coupled Fe–Fe pairs on the Sb-segregated surface, and the coordination geometry makes it impossible to assign antiparallel spin orientations to all pairs. Fig. 3 shows two different possibilities for spin orientations in which the preference for antiparallel orientation is satisfied for (a) all vertical pairs and (b) all diagonal pairs. We calculated the energies for these two cases and found that (a) is of lower energy than (b) by 0.024 eV per cell. Therefore, in the remaining calculations, we used the spin arrangement (a), in which the total difference between the numbers of α and β electrons is 5, as it is for the nonsegregated surface.

2.3. Calculation of surface free energies

The methodology for interpreting ab initio calculations of surface models in terms of the oxidation–reduction thermodynamics of the surface was first described by Scheffler and co-workers [42,43]. Here we summarize the main equations as applied to $FeSbO_4$. The most stable surface composition and geometry at a given temperature T and pressure p are those that minimize the thermodynamic potential,

$$\Phi(T, p, \mu_{Fe}, \mu_{Sb}, \mu_O) = G_{slab}(T, p) - \mu_{Fe}N_{Fe} - \mu_{Sb}N_{Sb} - \mu_O N_O, \quad (1)$$

where G_{slab} is the Gibbs free energy of the slab and μ_x ($x = $ Fe, Sb, O) are the chemical potentials of the different species, which are not independent from each other, because the equilibrium condition requires that

$$\mu_{Fe} + \mu_{Sb} + 4\mu_O = g_{bulk}, \quad (2)$$

where g_{bulk} is Gibbs free energy *per formula unit* for the $FeSbO_4$ bulk. If we limit our discussion to slabs with Sb/Fe = 1 ($N_{Fe} = N_{Sb}$), then the potential Φ can be expressed as a function of the oxygen chemical potential,

$$\Phi = G_{slab} - G_{bulk} - (N_O - 4N_{Fe})\mu_O, \quad (3)$$

where $G_{bulk} = N_{Fe}g_{bulk}$ is the Gibbs free energy of the portion of the bulk with the same number of Fe (and Sb) atoms as the slab. It is convenient at this point to divide the equation by the surface area A of the slab (including a factor of 2 to account for both the bottom and the top surfaces), which defines the potential per unit surface σ as

$$\sigma \equiv \frac{\Phi}{2A} = \frac{G_{slab} - G_{bulk}}{2A} - \frac{\Gamma_O}{A}\mu_O, \quad (4)$$

where $\Gamma_O = \frac{1}{2}(N_O - 4N_{Fe})$ is the excess of oxygen at each surface of the slab. Following other authors [38,42,43], we now approximate the difference in free energies by the difference between calculated energies for the slab and the bulk. Because the oxygen chemical potential is a function of temperature and pressure (or, more precisely, the partial pressure of O_2 in the gas phase), we can write

$$\sigma(T, p) = \frac{E_{slab} - E_{bulk}}{2A} - \frac{\Gamma_O}{A}\mu_O(T, p). \quad (5)$$

For the stoichiometric composition ($\Gamma_O = 0$) the thermodynamic potential per area unit $\sigma(T, p)$, which is usually called the surface free energy, becomes just the surface energy,

$$\sigma|_{\Gamma_O=0} = \gamma \equiv \frac{E_{slab} - E_{bulk}}{2A}. \quad (6)$$

But on increasing $\mu_O(T, p)$, by increasing the O_2 partial pressure or by lowering the temperature, the surfaces with oxygen excess ($\Gamma_O > 0$) will have a lower surface free energy and become more favorable, whereas the surfaces with oxygen deficiency ($\Gamma_O < 0$) will have a higher surface free energy and become less stable.

We now need to know the pressure and temperature dependence of the chemical potential of oxygen in a gas of O_2 molecules. Assuming that the gas is ideal, the variation of the chemical potential with pressure is given by

$$\mu_O(T, p) = \mu_O(T, p_0) + \frac{1}{2}kT \ln\frac{p}{p_0}, \quad (7)$$

where p_0 is a reference pressure for which the chemical potential variation with temperature $\mu_O(T, p_0)$ is known (here $p_0 = 1$ bar). $\mu_O(T, p_0)$ can be decomposed into two terms,

$$\mu_O(T, p_0) = \frac{1}{2}E[O_2] + \frac{1}{2}\Delta g_{O_2}(T, p_0). \quad (8)$$

The first term is the 0 K contribution, which is approximated here as the calculated energy of the oxygen molecule (zero point vibration contributions are ignored). The second term is the difference in the Gibbs free energy per O_2 molecule between 0 K and T, at constant pressure p_0, which is related to the enthalpy h and entropy s of the O_2 gas as

$$\Delta g_{O_2}(T, p_0) = h(T, p_0) - h(0\text{ K}, p_0) - Ts(T, p_0). \quad (9)$$

The values of h and s have been tabulated in thermochemical tables [44] for different temperatures and $p_0 = 1$ bar; the full dependence of the chemical potential with pressure and temperature is known. It is common to express the chemical potential taking one-half of the energy of the O_2 molecule as a reference,

$$\mu_O(T, p_0) - \frac{1}{2}E[O_2] \to \mu_O(T, p_0). \quad (10)$$

We use the same convention here, but it is important to note that this convention implies that the slab energies used to calculate the surface free energies should be corrected in the same way; that is, the energy $\frac{1}{2}E[O_2]$ should be subtracted for each oxygen atom in the slab.

The energy of the O_2 molecule was obtained with VASP for the same oxygen PAW potential as in the $FeSbO_4$ calculations (see Ref. [22]). We calculated an equilibrium bond distance of 1.235 Å (compared with the experimental value of 1.207 Å) and a spin triplet solution corresponding to an energy $E[O_2]$ of −9.826 eV. This energy should not be compared directly with the dissociation energy of the oxygen molecule, because it was calculated with reference to a nonmagnetic state of the oxygen atom, which is not the correct ground state; however, the atom energy reference is irrelevant for our results, because it cancels out in all energy differences.

3. Results and discussion

3.1. Stoichiometric surfaces

We first consider the case where the surface model keeps the stoichiometric composition of the bulk, that is, the slab has an exact number of $FeSbO_4$ formula units. In this case, either the two cations in the surface are both coordinatively unsaturated, with coordination to five oxygen anions (one less than in the bulk octahedra), or one cation has the full octahedral coordination, while the other is coordinated to only four oxygen atoms. A terminating oxygen atom can be either mono-coordinated to one of the cations or in a bridging position between two cations. Below we discuss the stability of different terminations, as well as the surface energy and relaxation for each cationic configuration.

We first consider the stoichiometric *unsegregated* surface. To investigate the relative stabilities of the different terminations, we relaxed the structure starting from four different arrangements of the surface oxygen positions, as shown in Fig. 4: (a) two oxygen atoms in bridging positions, (b) one oxygen mono-coordinated to Fe and the other mono-coordinated to Sb, (c) one oxygen in a bridging position and the other mono-coordinated to Sb, and (d) one oxygen in a bridging position and the other mono-coordinated to Fe. After relaxation, we found only two

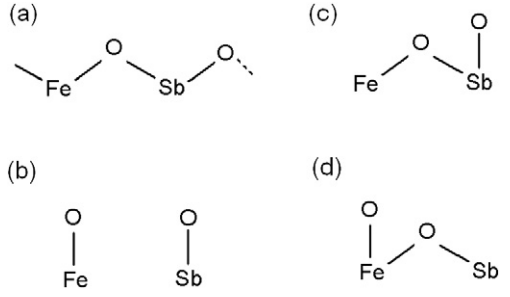

Fig. 4. Different terminations for the stoichiometric 100 surface: (a) two oxygen atoms in bridging positions, (b) one oxygen mono-coordinated to Fe and one mono-coordinated to Sb, (c) one oxygen in a bridging position and the other mono-coordinated to Sb, and (d) one oxygen in a bridging position and the other mono-coordinated to Fe.

different geometries: one with the two oxygen atoms in bridging positions (as in Fig. 4a), with a slab energy of −190.71 eV (the configurations shown in Figs. 4b and 4d relaxed to this configuration as well), and the other with one bridging oxygen and one oxygen atom mono-coordinated to Sb (Fig. 4c), but ∼4 eV higher in energy. Thus, clearly the stable termination for the stoichiometric surface is that with all of the oxygen atoms in bridging positions, where each cation at the surface is coordinated to five oxygen atoms.

Geometry optimization of the most stable configuration resulted in a weak surface relaxation, with only the bridging oxygen atoms changing their positions appreciably. Fe–O distances decreased from 2.08 and 2.00 Å to 1.94 and 1.92 Å, respectively, while Sb–O distances decreased from 2.02 and 1.98 Å to 1.94 and 1.95 Å, respectively, widening the Fe–O (bridging)–Sb angles from 99.1° and 102.4° to 104.9° and 109.1°, respectively. The plane of these bridges was rotated slightly compared with the bulk, moving the bridging oxygen toward the position of the missing oxygen atoms in the incomplete surface octahedra. This rotation changed the O–Fe–O angles from nearly 90°, corresponding to the bulk octahedra (88.1° and 91.8°), to 102.8° and 102.3°, respectively, and changed the O–Sb–O angle from 91.1° and 91.8° to 100.0° and 102.3°, respectively. The surface energy was calculated at $\gamma = 63.5\ \mathrm{meV\,Å^{-2}} = 1.02\ \mathrm{J\,m^{-2}}$, which is relatively low, in agreement with the observation of the (100) surface in mineral samples.

We followed a similar procedure to investigate the stability of the different oxygen terminations in the stoichiometric surface with Sb segregated to the surface. In this case, the most stable termination was again that with the two oxygen atoms in bridging positions, now forming Sb–O–Sb bridges. All of the other terminations explored were found to be unstable; after relaxation, they also converged to the stable termination with bridging oxygens.

The relaxed Sb–O distances along the bridges were 2.03 Å, nearly 0.1 Å longer than the corresponding Sb–O distances in the unsegregated surface. The bridging position and the long distances are inconsistent with the hypothesis of covalent double bonds being formed in the surface, which has been suggested by Sala and Trifiro [9] and Carbucicchio et al. [10] as an explanation for the higher selectivity of Sb-enriched surfaces. This finding is another indication that the Sb–O interaction in this antimonate is less covalent than often assumed and has a relatively high ionic character, as we found in an earlier computer modeling study of the electronic structure of this oxide [37].

The slab energy for the most stable termination in this case was −189.205 eV, which corresponds to a surface energy of $\gamma = 89.3\ \mathrm{meV\,Å^{-2}} = 1.43\ \mathrm{J\,m^{-2}}$. This value is higher than the surface energy of the slab with a bulk-like distribution of cations, showing that the segregation of the Sb cations to the (100) surface is not thermodynamically favorable. Note, however, that the actual composition of the surface can be affected by a number of factors, including pressure and temperature, as discussed later. Furthermore, the composition of the surface is likely to be kinetically controlled and dependent on the synthesis conditions. Berry et al. [41], for example, have shown that

Table 1
Slab energies (E_{slab}) and surface energies (γ) for the different cation distributions in the stoichiometric (100) surface

	Bulk-like	Sb segregated	Fe segregated
E_{slab} (eV)	−190.71	−189.20	−188.59
γ (J m^{-2})	1.02	1.43	1.60

iron antimonate formed in a sealed tube with an excess of antimony oxide reactants has an Sb-enriched surface, which they attribute to the incomplete volatilization of excess antimony oxide. Therefore, in what follows we consider both the bulk-like surface and the Sb-segregated surface in our calculations.

Finally, for the sake of comparison, we also calculated an Fe-segregated surface model in which Fe cations are in the surface layer and Sb cations are in the subsurface layer. The slab energy in this case was −188.59 eV, which is 2.12 eV higher than for the bulk-like surface and 0.61 eV higher than for the Sb-segregated surface. The corresponding surface energy was $\gamma = 99.8$ meV Å^{-2} $= 1.60$ J m^{-2}, and we did not investigate this surface any further. To the best of our knowledge, the existence of Fe-rich surfaces in $FeSbO_4$ has not been reported in experimental studies. The slab and surface energies for all of the different cation distributions in the surface are summarized in Table 1.

3.2. Surface reduction

We can calculate the vacancy formation energies (*VFE*s) for the surface by removing one of the terminal oxygen atoms from each surface of the stoichiometric slab,

$$VFE = \frac{1}{2}\left(E[O_2] + E_{slab}^{\Gamma_O=-1} - E_{slab}^{\Gamma_O=0}\right), \tag{11}$$

where in the superscript for the slab energies, we indicate the number Γ_O of oxygen atoms in excess at each surface of the slab with respect to the stoichiometric composition, and $E[O_2] = -9.826$ eV is the calculated energy of the oxygen molecule.

We first discuss the case of an oxygen vacancy at the unsegregated surface with a bulk-like distribution of cations (Fig. 5). The two bridging oxygen anions are not identical and thus have different *VFE* values. They correspond to bulk oxygen positions with different cation coordination; the coordination numbers to Sb ions are $Z_{Sb} = 1$ in one case and $Z_{Sb} = 2$ in the other, when the atoms are in the bulk. However, because of the presence of the surface, they lose one coordination to Fe or to Sb, respectively, and their immediate coordination is now the same—that is, they both are coordinated to one Sb and one Fe. Still, they have different *VFE*s: 1.36 eV and 1.22 eV, respectively, due to the ordering of the Fe and Sb cations in the subsurface layers along the [100] direction. Because, according to previous studies in the $FeSbO_4$ bulk, cations can be disordered in that direction, a range of *VFE*s around these two values should be expected for the actual surface. The calculated formation energies of the surface oxygen vacancies are significantly low, suggesting that considerable oxygen depletion at the surface is likely at high temperatures, a point discussed in more detail

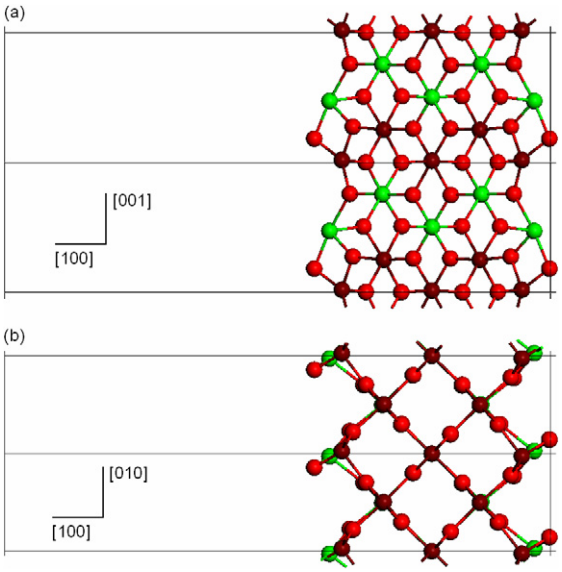

Fig. 5. Relaxed geometry for the unsegregated surface with one oxygen vacancy. (a) View along the [010] direction; (b) view along the [001] direction. Red, brown and green represent oxygen, iron and antimony, respectively. (For interpretation of the references to colour in this figure legend, the reader is referred to the web of this article.)

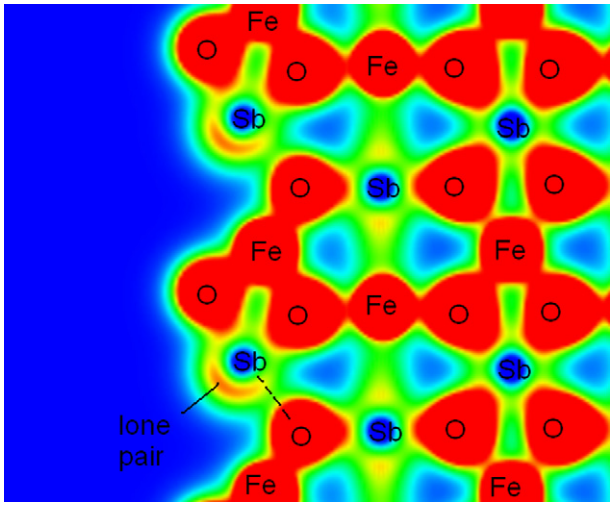

Fig. 6. Electron density plot in a plane intersecting the bulk-like (100) surface with an oxygen vacancy. The dashed line represents the longest Sb–O distance around the Sb^{3+} cation.

below. The surface *VFE*s are much lower than the calculated values for the bulk vacancies (2.26–3.46 eV) reported previously [22], which means that any oxygen vacancies will tend to accumulate at the surface of the material.

The creation of neutral oxygen vacancies in the surface introduces the question of the location of the two electrons left behind by the removed oxygen. Fig. 6 plots the electron density in the plane of the Sb–O–Fe bridges. Just as with the bulk oxygen vacancies described previously [22], the electrons appear to locate at the antimony site, forming an Sb^{3+} cation with a lone pair pointing to the vacancy site.

Additional evidence for the formation of an Sb^{3+} cation is provided by the average Sb–O distance, which increases with

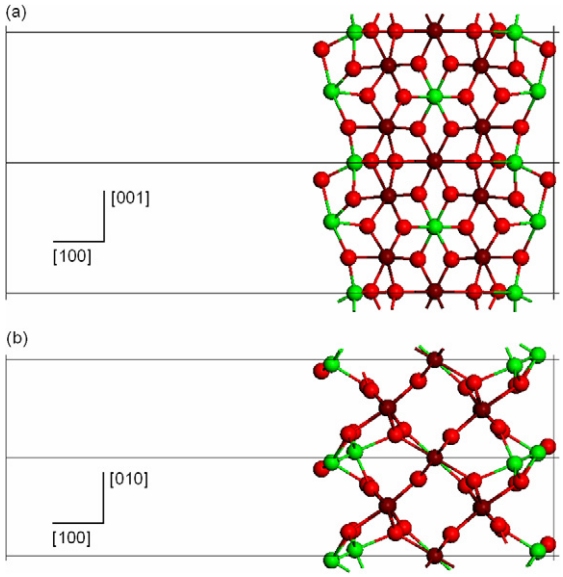

Fig. 7. Sb-segregated (100) surface with one oxygen vacancy per supercell. The positions of the atoms are relaxed. (a) View along the [010] direction; (b) view along the [001] direction. Red, brown and green represent oxygen, iron and antimony, respectively. (For interpretation of the references to colour in this figure legend, the reader is referred to the web of this article.)

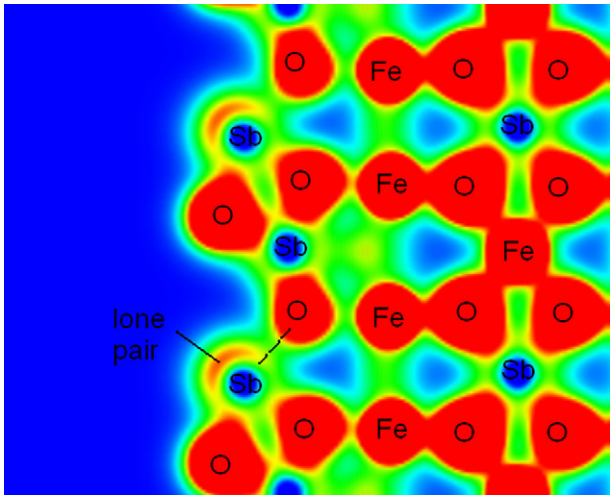

Fig. 8. Electron density plot in a plane intersecting the Sb-segregated (100) surface with an oxygen vacancy. The dashed line represents the longest Sb–O distance around the Sb^{3+} cation.

respect to the stoichiometric surface. But because the lone pair has a well-defined orientation, not all Sb–O distances increase equally; the distance to the O anion that was in the same shared edge as the removed oxygen increases the most (from 2.06 Å to 2.36 Å), because this oxygen anion is the closest to the lone pair (Fig. 6), whereas the rest of the Sb–O distances increase by 0.03–0.09 Å.

We also investigated the formation of oxygen vacancies in the Sb-segregated surface. We explored different oxygen terminations to find the lowest-energy configuration for this particular surface and found that much more surface relaxation occurred around the vacancy here (Fig. 7) than in the bulk-like surface. As shown in the charge density plot (Fig. 8), one of the surface Sb atoms receives the electron pair left behind by the oxygen, forming a lone-pair Sb^{3+} cation, while the other remains as Sb^{5+}. The relaxation around the Sb^{3+} cation was similar to that described for the bulk-like surface. Again, the distance to the O atom in the same shared edge as the abstracted oxygen increased the most (from 2.04 to 2.33 Å), because this oxygen anion was the one that was most repelled by the lone pair. The rest of the Sb^{3+}–O^{2-} distances increased by 0.02–0.12 Å.

The most important differences between this surface and the bulk-like surface are introduced by the presence in the reduced surface of a coordinatively unsaturated Sb^{5+} cation. Around the unrelaxed vacancy, this cation was coordinated to only four oxygen atoms, with both of the two dangling bonds pointing outward from the surface. This uneven distribution of the coordination directions was much less favorable for the Sb^{5+} cation in this surface than it was for the more ionic Fe^{3+} cation in the bulk-like reduced surface. Consequently, the Sb^{5+} relaxed strongly, moving inward to reach a more even coordination distribution, thereby gaining an increased coordination from one of the oxygen atoms in the subsurface layers (Fig. 7). The more drastic relaxation of the Sb^{5+} cation in this surface compared with the relaxation of the Fe^{3+} cation in the bulk-like surface also could be favored by the higher charge on the Sb^{5+} cation, which causes a stronger electrostatic force from the subsurface oxygen anions.

As a consequence of this surface relaxation, the energy required to create the vacancy in the Sb-segregated surface, which, on the basis of the arguments presented previously [22], would be expected to be higher than the *VFE* for the bulk-like surface, was actually lower (1.03 eV). It is possible to question this result by arguing that because of the severe relaxation described above, the slab model may not be of sufficient thickness to prevent a coupling between the relaxations of the two surfaces of the slab, and thus the low *VFE* might be an artifact introduced by this interaction. To clarify this point, we recalculated the *VFE* using a thicker slab, with seven octahedral layers; the result (1.00 eV) is very close to that obtained with the five-layer model, and thus we can conclude that the result is little affected by the thickness of the slab.

Although the relative energy of the reduced surface, calculated with respect to the corresponding parent surface, was lower for the Sb-segregated surface than for the unsegregated surface, the total energy of the reduced slab was still higher for the Sb-segregated surface. Therefore, the oxygen vacancy formation and surface reduction cannot be the cause of the segregation of Sb to the surface.

We now consider the possibility of the formation of a second oxygen vacancy at each side of the slab. In the present supercell model, this second vacancy implies the complete reduction of the surfaces, where two electron pairs are left behind by the removed oxygen atoms. We first discuss the surface without cation segregation (Fig. 9). As in the previous cases, two electrons localize as a lone pair on the surface Sb, forming a Sb^{3+} cation. The other cation in the surface is an Fe^{3+}, which generally can accept only one electron, and thus the second electron

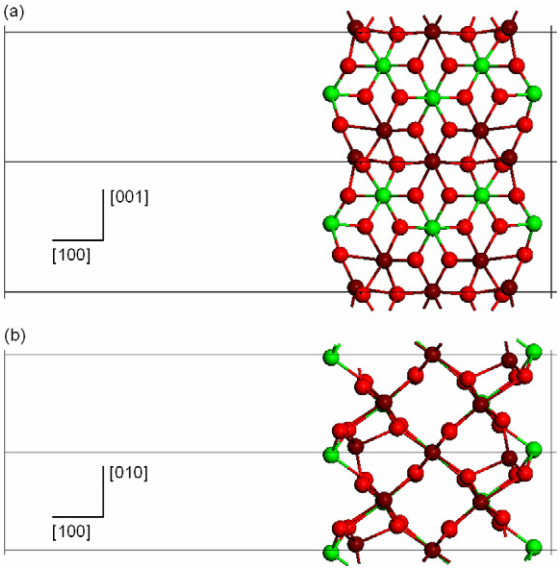

Fig. 9. Completely reduced (100) surface without cation segregation. (a) View along the [010] direction; (b) view along the [001] direction. Red, brown and green represent oxygen, iron and antimony, respectively. (For interpretation of the references to colour in this figure legend, the reader is referred to the web of this article.)

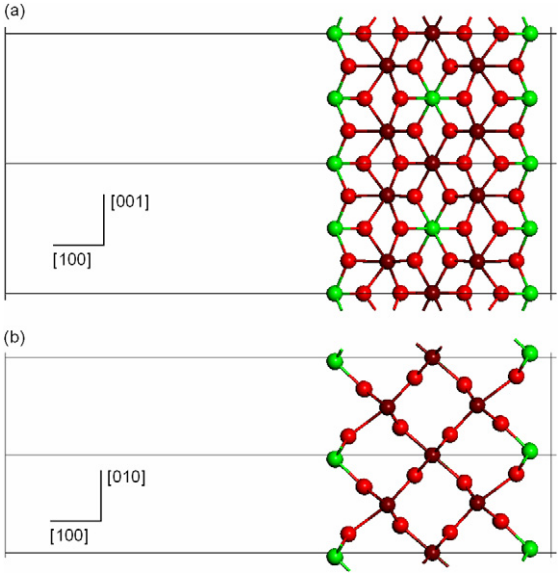

Fig. 10. Completely reduced surface with Sb segregation. (a) View along the [010] direction; (b) view along the [001] direction. Red, brown and green represent oxygen, iron and antimony, respectively. (For interpretation of the references to colour in this figure legend, the reader is referred to the web of this article.

pair becomes distributed between one Fe^{3+} ion in the surface and one in the subsurface layer, thus forming two Fe^{2+} cations.

This electronic redistribution is confirmed by the examination of the spin density around the Fe cations in the surface and subsurface layers. The spin population inside an integration sphere of radius 1.30 Å decreased from 4.24 in the bulk to 3.68, suggesting a reduction from high-spin Fe^{3+} to high-spin Fe^{2+}. The magnetization of the slab (the difference between the total numbers of spin-up and spin-down electrons in the cell) did not change on reduction of the iron cations, because the spin population on Fe has opposite signs in the surface and the subsurface layers for the antiferromagnetic model used here. We repeated the calculation with ferromagnetic ordering of the spin moments; as expected, the magnetization decreased by 4 with respect to the stoichiometric surface, demonstrating a reduction of 4 Fe cations (2 at each slab surface). The energy for this ferromagnetic configuration was higher than that for the antiferromagnetic case, demonstrating that no change in magnetic ordering occurred on surface reduction.

In the relaxed surface, the surface Fe^{2+} cation moved inward extensively (by ∼1 Å) and actually gained an extra coordination to an oxygen atom underneath the subsurface layer of cations (Fig. 9). In this new position, the Fe^{2+} cation had a distorted tetrahedral coordination. The Sb^{3+} cation was also tetrahedrally coordinated if the lone pair was counted as a coordinating species, preventing strong relaxation of this cation.

The large relaxations on the totally reduced surface stabilizes this surface composition and makes the formation of the second vacancy no more energetically unfavorable than the first vacancy. The energy of formation of the second vacancy for the bulk-like surface, calculated with respect to the most stable partially reduced surface,

$$VFE' = \frac{1}{2}\left(E[O_2] + E_{\text{slab}}^{\Gamma_O=-2} - E_{\text{slab}}^{\Gamma_O=-1}\right), \tag{12}$$

was 1.21 eV.

The total reduction of the Sb-segregated surface produced a more symmetric surface (Fig. 10) with much less relaxation of the subsurface layers than in the unsegregated surface. In this case, the two cations in the surface were both reduced antimony species Sb^{3+}, and the formation energy of the second vacancy, calculated with respect to the most stable Sb-segregated surface with one vacancy, was 1.27 eV.

3.3. Surface oxidation

Along with the reduction of bulk-like and segregated surfaces, we also investigated surface oxidation, by exploring several configurations for adsorption of an extra oxygen atom ($\Gamma_O = 1$) at the surfaces. To find the minimum energy configuration for the adsorption, we generated different initial geometries, which we then relaxed.

In the case of the unsegregated surface, the most stable configuration is shown in Fig. 11. One of the oxygen atoms in the surface is in a bridging position as in the stoichiometric surface, while the other two atoms resemble an adsorbed O_2 species, in a bridging position between Fe and Sb [d(Fe–O) = 1.88 Å and d(Sb–O) = 2.02 Å]. The magnetization per cell in the final solution is the same as in the stoichiometric surface, and no spin density is found around the oxygen atoms, demonstrating that the adsorbed species is in a singlet state, like the peroxy O_2^{2-} ion, and not a triplet like the neutral oxygen molecule. The calculated O–O distance of 1.40 Å is close to the O–O distance of 1.44 Å calculated by other authors for the peroxy species

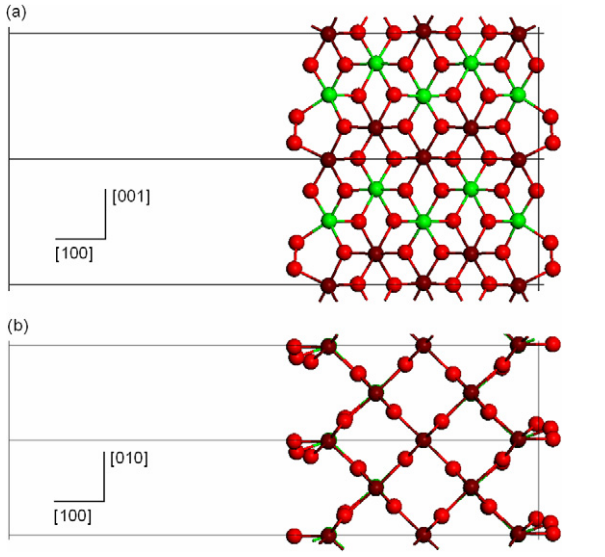

Fig. 11. Geometry of the oxidized slab with no cation segregation. There is one oxygen atom in excess at each surface. (a) View along the [010] direction; (b) view along the [001] direction. Red, brown and green represent oxygen, iron and antimony, respectively. (For interpretation of the references to colour in this figure legend, the reader is referred to the web of this article.

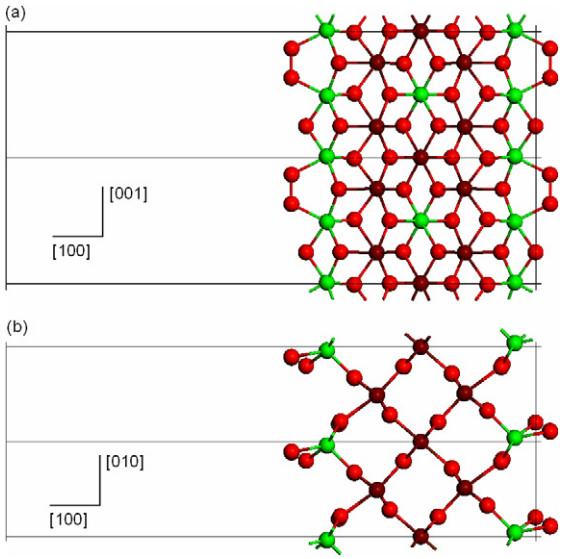

Fig. 12. Geometry of the oxidized Sb-segregated surface, with one oxygen atom in excess at each surface. (a) View along the [010] direction; (b) view along the [001] direction. Red, brown and green represent oxygen, iron and antimony, respectively. (For interpretation of the references to colour in this figure legend, the reader is referred to the web of this article.)

adsorbed at the (010) surface of MoO_3 [45] as well as to the experimental O–O distance of the peroxy ion in hydrogen peroxide (1.475 Å) [46].

All of the other configurations investigated for this surface composition were found to be less stable than the one described above, with energy differences >1 eV. In particular, an O_2 species perpendicular to the surface corresponds to an energy 1.1 eV higher than the most stable configuration, in which the O–O is nearly parallel to the surface.

The atomic adsorption energy, defined as the energy required to take one oxygen atom from an oxygen molecule and adsorb it onto the surface, can be calculated for the most stable adsorption configuration as

$$E_{\text{ads}}^{\text{O}} = \frac{1}{2}E_{\text{slab}}^{\Gamma_{\text{O}}=1} - \frac{1}{2}E_{\text{slab}}^{\Gamma_{\text{O}}=0} - \frac{1}{2}E[\text{O}_2]. \tag{13}$$

A negative value of the adsorption energy means that the oxidized surface is thermodynamically favorable at 0 K with respect to the stoichiometric surface, although in general its stability at finite temperatures will depend on the temperature as well as on the partial pressure of oxygen in the surrounding atmosphere, as discussed in the next section. But in our case, we obtained a positive value (0.99 eV) of the adsorption energy, which means that the oxidized surface cannot be thermodynamically stable with respect to the stoichiometric surface at any temperature.

Nonetheless, it should be noticed that the oxidized surface is stable with respect to the surface with one oxygen vacancy plus an isolated oxygen molecule. Even when the most stable reduced surface is considered, the calculated adsorption energy of the oxygen molecule on the vacancy,

$$E_{\text{ads}}^{\text{O}_2} = \frac{1}{2}E_{\text{slab}}^{\Gamma_{\text{O}}=1} - \frac{1}{2}E_{\text{slab}}^{\Gamma_{\text{O}}=-1} - E[\text{O}_2], \tag{14}$$

is negative (−0.23 eV). Therefore, adsorption of oxygen can occur as part of the dynamical process of oxidation reduction of the surface, in which the metastable surface configuration with $\Gamma_{\text{O}} = 1$ (the O_2^{2-} species) can form as the result of the adsorption of one O_2 molecule at an oxygen vacancy in the surface. This adsorption restores the original oxidation states of the cations around the vacancy; that is, the reduced Sb^{3+} cation transfers its lone pair of electrons to the oxygen molecule. The nondefective surface can then be restored if the O_2^{2-} species dissociates and one of the oxygen atoms diffuses to fill a neighboring oxygen vacancy.

On the Sb-segregated surface, the adsorption of one oxygen atom again led to the formation of a surface peroxy group in a bridging position (Fig. 12) with d(O–O) = 1.45 Å, which is slightly longer than in the Fe–O–O–Sb case. Again, the configuration with an O_2 species perpendicular to the surface was considerably less stable. For the peroxy in a bridging position, the two Sb–O distances were equal (2.00 Å) and similar to the Sb–O distances in the bulk. The adsorption energy of an atom in the stoichiometric surface was still positive ($E_{\text{ads}}^{\text{O}} = 0.80$ eV), but somewhat lower than that for the unsegregated surface. The difference in the adsorption energies between the two surfaces is not sufficient to favor the oxidized Sb-segregated energy with respect to the unsegregated surface, because the total energy of the former slab is still higher (by 1.1 eV). On the other hand, the adsorption energy of the molecule at a vacancy site at the segregated surface is also negative and of the same value as in the bulk-like surface ($E_{\text{ads}}^{\text{O}_2} = -0.23$ eV). The value is not more negative than in the bulk-like surface, because the formation energy of the vacancy is slightly higher at the segregated surface, as reported above.

To complete our study of surface oxidation, we investigated the possibility of the adsorption of a second oxygen atom at

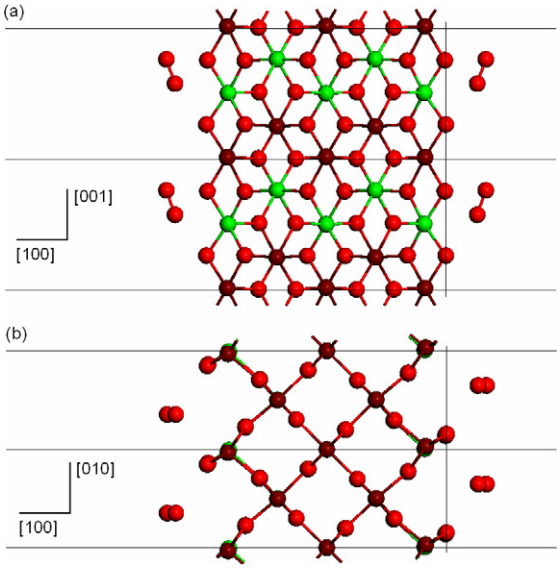

Fig. 13. Relaxed geometry for the surface with composition $\Gamma_O = 2$, in which an oxygen molecule has desorbed from the surface. (a) View along the [010] direction; (b) view along the [001] direction. Red, brown and green represent oxygen, iron and antimony, respectively. (For interpretation of the references to colour in this figure legend, the reader is referred to the web of this article.)

each surface per unit cell ($\Gamma_O = 2$), leading to fully oxidized surfaces. For the unsegregated surface, we found that, starting from any adsorption configuration for the two additional oxygen atoms, an oxygen molecule almost desorbed from the surface in the final structure (Fig. 13). It should be stressed that the present situation, in which no local minimum could be found corresponding to the additional oxygen atoms forming surface species, differs from the case of the adsorption of one oxygen atom discussed above, because in that case a local minimum could be found corresponding to the formation of a peroxy species.

The O_2 species shown in Fig. 13 has 2 unpaired electrons (triplet) and $d(\text{O–O}) = 1.23$ Å, which correspond to the experimental and calculated ground state of a neutral oxygen molecule. The calculated adsorption energy of only −23 meV with respect to the stoichiometric surface confirms that this molecule is only very weakly physisorbed at the surface, and thus it will completely desorb to the gas phase even at relatively low temperatures. The shortest distances from the oxygen atoms in the molecule to the cations in the surfaces were $d(\text{Sb–O}) = 3.07$ Å and $d(\text{Fe–O}) = 3.751$ Å. In the Sb-segregated surface, our calculations failed to find a local minimum for adsorption for this composition.

3.4. Temperature and pressure effects

Based on the results of the calculations, we can plot the dependence of the surface free energies, σ, on the oxygen chemical potential, μ_O, for each surface composition, following the approximations explained in Section 2. Figs. 14a and 14b show the results for the unsegregated and the Sb-segregated surfaces, respectively, and Fig. 14c illustrates the relationship between

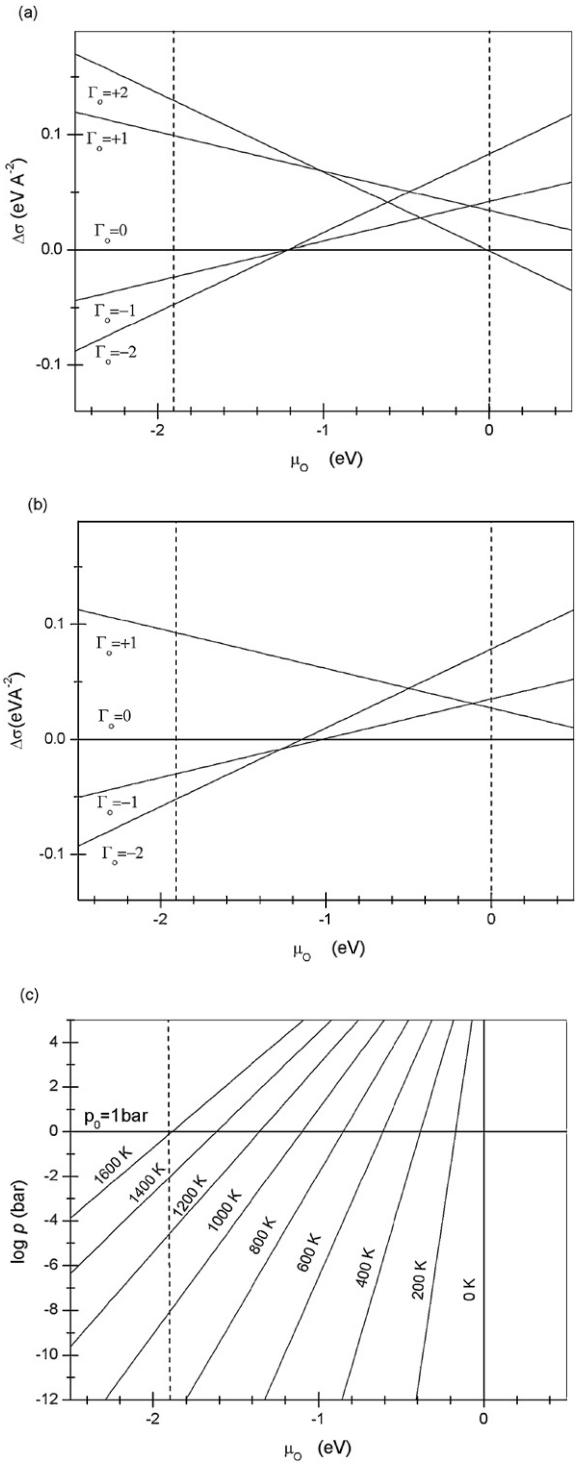

Fig. 14. Surface free energies (relative to the stoichiometric surfaces) for different terminations of (a) the unsegregated surface and (b) the Sb-segregated surface. Plot (c) shows the relationship between the chemical potential and oxygen partial pressure and temperature.

the chemical potential and the temperature and oxygen partial pressure. High chemical potentials, which favor the oxidation of surfaces, correspond to low temperatures and/or high oxygen partial pressures, whereas low chemical potentials, which favor the reduction of surfaces, correspond to high temperatures and/or low oxygen partial pressures.

It is important to note that experimentally, the chemical potential can be varied only within limits. If the chemical potential is too low, then too much oxygen will leave the sample, and the oxide will decompose to a different phase with cations in lower oxidation states or will be completely reduced. We estimated the lower limit of the chemical potential based on the experimental work of Walczak et al. [47], who found that the $FeSbO_4$ phase in ambient air is stable up to ∼1543 K. Considering that in atmospheric air, the oxygen partial pressure is ∼0.21 bar, it is easy to check that the corresponding chemical potential is ∼−1.9 eV, which we use as the lower boundary value. In contrast, the vertical line at 0 K marks a higher limit for the chemical potential, $\mu_O = 0$ eV. This is only a well-defined theoretical limit, because in principle at very high pressures, the chemical potentials at finite temperatures can exceed this value. However, most of the experimental data available refer to studies at the order of the atmospheric pressure (∼1 bar), and thus such high pressures are not of primary interest here. Consequently, we restrict our analysis to -1.9 eV $< \mu_O < 0$ eV; this range of chemical potentials is marked by two vertical lines in the figures.

The plots of σ versus μ_O in Fig. 14 show the relative stabilities of the surface terminations that we considered in this study: the stoichiometric termination ($\Gamma_O = 0$), 50% reduced surface ($\Gamma_O = -1$), 100% reduced surface ($\Gamma_O = -2$), 50% oxidized surface ($\Gamma_O = 1$), and 100% oxidized surface ($\Gamma_O = 2$). We restricted our study to these terminations because of the limitations imposed by the size of the simulation cell; of course, this does not mean that the surface composition is restricted in any way to these discrete values. Our approach should be seen as just a convenient (and rather rough) discretization of the continuous variation of the surface composition on changes in the gas-phase chemical potential. The stoichiometric composition of the surface is the most stable of the terminations studied over a wide range of temperature and pressure conditions. In atmospheric air, for example, where the partial pressure of oxygen is ∼0.21 bar, the stoichiometric termination is stable with respect to the reduced surfaces up to ∼1020 K for the unsegregated surface, and up to ∼900 K for the Sb-segregated surface. The second temperature is lower because, as discussed above, the strong relaxation of the Sb-segregated surface on the creation of oxygen vacancies stabilizes that reduced surface termination. The reduced surfaces with $\Gamma_O = -1$ or $\Gamma_O = -2$ also can be stabilized with respect to the stoichiometric termination at much lower temperatures, if vacuum pressures are applied. At ultra-high vacuum (UHV) conditions (e.g., 10^{-12} bar), the stoichiometric composition is the most stable only up to ∼550 K for the nonsegregated surface and ∼460 K for the Sb-segregated surface.

The range of chemical potentials at which the stoichiometric surface is the most stable includes the typical temperatures and pressures of the industrial catalytic process (700–750 K and ∼1 bar for propene ammoxidation [48]). Of course, oxygen vacancies can also be formed in this range of chemical potentials. The above results indicate the stability of the stoichiometric surface only with respect to heavily reduced surfaces (50–100% of surface oxygen desorbed); however, partially reduced surfaces with lower vacancy concentrations can be stable at relatively low temperatures.

In contrast, the oxidized surfaces with >50% of overstoichiometric oxygen covering are only metastable in the complete range of temperatures and pressures, as predicted previously from the positive values of the adsorption energies. The difficulty in oxidizing the surface arises from the fact that the cations in $FeSbO_4$ are already in their maximum oxidation states, which prevents the reduction of molecular oxygen at the surface. Thus the adsorption of molecular oxygen as a peroxy ion will probably occur at an oxygen vacancy site near a Sb^{3+}, which can donate its lone pair to form the peroxy species. As discussed in the previous section, our results suggest that the peroxy ion will dissociate and one of the oxygen atoms will diffuse to a neighboring vacancy where it can form an O^{2-} species. This mechanism seems to be more favorable than the absorption of O_2 at each vacancy site, since even at very low temperatures and relatively high partial pressures of oxygen the stoichiometric composition of the surface is thermodynamically favorable.

4. Conclusion

In the present work, we have investigated the properties of the (100) surface of iron antimonate $FeSbO_4$. We calculated the geometries and stabilities of different surface compositions, including two different distributions of cations, a bulk-like distribution with Fe and Sb alternation in the [001] direction, and an Sb-segregated distribution. We showed that the introduction of oxygen vacancies led to the formation of Sb^{3+} species in the surface, with lone pairs pointing at the vacancy site. Only when no Sb^{5+} cations were present for reduction did the electrons go to iron to form Fe^{2+} species, a behavior similar to that of the bulk material when oxygen vacancies are introduced. Because each Fe^{3+} cation can accept only one electron, this process can involve the reduction of iron species in the subsurface layers. The formation of oxygen vacancies was slightly more favorable in the Sb-segregated surface than in the unsegregated surface because of the strong relaxation on vacancy formation which occurs by the former. The ordered surface, however, remained more stable in all cases.

Our analysis of the variation of the free energies of the surfaces with temperature and oxygen partial pressure suggests that for both surface distributions of cations, the stoichiometric composition of the surface is stable in a wide range of temperature and pressure conditions. Partially or totally reduced surfaces became more favorable than stoichiometric surfaces at temperatures near 1000 K for samples in atmospheric air. Molecular oxygen could adsorb at an oxygen vacancy in the form of a peroxy ion, accepting two electrons from the reduced Sb^{3+} cation near the vacancy. The resulting structure is of higher energy than the combination of an atom in a gas-phase molecule plus the stoichiometric slab. These metastable species probably dissociate to fill neighboring vacancy sites, keeping the stoichiometric composition of the surface. Overall, the present investigation has enhanced our understanding of surface redox processes in this widely used catalytic material.

Acknowledgments

This work was supported by the EPSRC under Grant GR/S01986/01. Computer resources on HPCx were provided by the Materials Chemistry HPC Consortium and funded by the EPSRC (portfolio Grant EP/D504872/1). The authors thank Dr. Alexey A. Sokol for useful discussions.

References

[1] G.W. Keulks, M.Y. Lo, Abstr. Pap. Am. Chem. Soc. 187 (1984) 24.
[2] G.W. Keulks, M.Y. Lo, J. Phys. Chem. 90 (1986) 4768.
[3] M.D. Allen, M. Bowker, Catal. Lett. 33 (1995) 269.
[4] M. Allen, R. Betteley, M. Bowker, G.J. Hutchings, Catal. Today 9 (1991) 97.
[5] M. Bowker, C.R. Bicknell, P. Kerwin, Appl. Catal. A 136 (1996) 205.
[6] R.K. Grasselli, Top. Catal. 21 (2002) 79.
[7] G.K. Boreskov, S.A. Veniaminov, V.A. Dzisko, D.V. Tarasova, V.M. Dindoin, N.M. Sanobova, I.P. Olenkova, L.M. Kefeil, Kinet. Katal. 10 (1969) 1530.
[8] T.V. Adamiya, Y.A. Mishchenko, D.A. Dulin, A.I. Gelbshtein, Kinet. Katal. 11 (1970) 1168.
[9] F. Sala, F. Trifiro, J. Catal. 41 (1976) 1.
[10] M. Carbucicchio, G. Centi, F. Trifiro, J. Catal. 91 (1985) 85.
[11] V. Fattore, Z.A. Fuhrman, G. Manara, B. Notari, J. Catal. 37 (1975) 223.
[12] I. Aso, S. Furukawa, N. Yamazoe, T. Seiyama, J. Catal. 64 (1980) 29.
[13] N. Burriesci, F. Garbassi, M. Petrera, G. Petrini, J. Chem. Soc. Faraday Trans. I 78 (1982) 817.
[14] R.G. Teller, J.F. Brazdil, R.K. Grasselli, W. Yelon, J. Chem. Soc. Faraday Trans. I 81 (1985) 1693.
[15] S.R.G. Carrazan, L. Cadus, P. Dieu, P. Ruiz, B. Delmon, Catal. Today 32 (1996) 311.
[16] E. van Steen, G. Kuwert, A. Naidoo, M. Williams, in: 3rd World Congress on Oxidation Catalysis, 1997, p. 423.
[17] G.A. Zenkovets, G.N. Kryukova, S.V. Tsybulya, Kinet. Catal. 43 (2002) 731.
[18] P. Berlepsch, T. Armbruster, J. Brugger, A.J. Criddle, S. Graeser, Mineral. Mag. 67 (2003) 31.
[19] R. Grau-Crespo, N.H. de Leeuw, C.R.A. Catlow, Chem. Mater. 16 (2004) 1954.
[20] X. Obradors, J. Bassas, J. Rodriguez, J. Pannetier, A. Labarta, J. Tejada, F.J. Berry, J. Phys. Condens. Matter 2 (1990) 6801.
[21] R. Grau-Crespo, N.H. de Leeuw, C.R.A. Catlow, J. Mater. Chem. 13 (2003) 2848.
[22] R. Grau-Crespo, I.D.R. Moreira, F. Illas, N.H. de Leeuw, C.R.A. Catlow, J. Mater. Chem. 16 (2006) 1943.
[23] P. Berlepsch, J. Brugger, Schweizer Strahler 11/9 (1999) 425.
[24] G. Kresse, J. Furthmuller, Comput. Mater. Sci. 6 (1996) 15.
[25] G. Kresse, J. Furthmuller, Phys. Rev. B 54 (1996) 11169.
[26] G. Kresse, J. Hafner, Phys. Rev. B 48 (1993) 13115.
[27] G. Kresse, J. Hafner, J. Phys. Condens. Matter 6 (1994) 8245.
[28] V.I. Anisimov, J. Zaanen, O.K. Andersen, Phys. Rev. B 44 (1991) 943.
[29] A. Rohrbach, J. Hafner, G. Kresse, J. Phys. Condens. Matter 15 (2003) 979.
[30] A.I. Liechtenstein, Phys. Rev. B 52 (1995) R5467.
[31] S.L. Dudarev, G.A. Botton, S.Y. Savrasov, C.J. Humphreys, A.P. Sutton, Phys. Rev. B 57 (1998) 1505.
[32] I.V. Solovyev, P.H. Dederichs, V.I. Anisimov, Phys. Rev. B 50 (1994) 16861.
[33] J.P. Perdew, A. Zunger, Phys. Rev. B 23 (1981) 5048.
[34] S.H. Vosko, L. Wilk, M. Nusair, Can. J. Phys. 58 (1980) 1200.
[35] J.P. Perdew, J.A. Chevary, S.H. Vosko, K.A. Jackson, M.R. Pederson, D.J. Singh, C. Fiolhais, Phys. Rev. B 46 (1992) 6671.
[36] C. Loschen, J. Carrasco, K.M. Neyman, F. Illas, Phys. Rev. B 75 (2007) 035115.
[37] R. Grau-Crespo, F. Cora, A.A. Sokol, N.H. de Leeuw, C.R.A. Catlow, Phys. Rev. B 73 (2006) 035116.
[38] A. Rohrbach, J. Hafner, G. Kresse, Phys. Rev. B 70 (2004) 125426.
[39] P.E. Blochl, Phys. Rev. B 50 (1994) 17953.
[40] G. Kresse, D. Joubert, Phys. Rev. B 59 (1999) 1758.
[41] F.J. Berry, J.G. Holden, M.H. Loretto, D.S. Urch, J. Chem. Soc. Dalton Trans. (1987) 1727.
[42] K. Reuter, M. Scheffler, Phys. Rev. B 65 (2002) 035406.
[43] X.G. Wang, W. Weiss, M. Shaikhutdinov, M. Ritter, F. Petersen, R. Wagner, R. Schlogl, M. Scheffler, Phys. Rev. Lett. 81 (1998) 1038.
[44] M.W.J. Chase, NIST-JANAF Thermochemical Tables, fourth ed., American Institute of Physics, New York, 1998.
[45] R. Coquet, D.J. Willock, Phys. Chem. Chem. Phys. 7 (2005) 3819.
[46] D.R. Lide, Handbook of Chemistry and Physics, 81 ed., CRC, London, 2000.
[47] J. Walczak, E. Filipek, M. Bosacka, Solid State Ionics 101 (1997) 1363.
[48] J. Hagen, Industrial Catalysis—A Practical Approach, Wiley–VCH, Weinheim, 1999.